Mar Biol (2015) 162:687–697
DOI 10.1007/s00227-015-2615-y

ORIGINAL PAPER

Shell growth, microstructure and composition over the development cycle of the European abalone *Haliotis tuberculata*

S. Auzoux-Bordenave · C. Brahmi · A. Badou · M. de Rafélis · S. Huchette

Received: 31 May 2014 / Accepted: 9 January 2015 / Published online: 22 January 2015

Abstract The shell of the European abalone *Haliotis tuberculata* is a model for studying mechanisms of mollusc shell formation, but the early steps of shell formation and calcification remain poorly documented. The microstructure and the mineralogical and geochemical composition of larval and juvenile shells were investigated by scanning electron microscopy, infrared spectroscopy and ion microprobe analyses (NanoSIMS). Analyses were performed on shells obtained from controlled fertilisations at the hatchery France-Haliotis (Plouguerneau, France) in July 2009 and 2010 using abalone from Roscoff. Shell cross sections revealed the microstructural arrangement of the developing shell, showing progressive biomineral organisation into two differentiated layers, i.e. the outer granular and the internal nacreous layer. Infrared analysis confirmed that the European abalone shell, at every stage of development, was mostly composed of $CaCO_3$ in the form of aragonite. Variations in trace element composition, i.e. Sr/Ca, were measured in the different stages and correlated with microstructural changes in the shells. Experimental manganese labelling of live abalones produced cathodoluminescence marks in the growing shell sections. The increase in shell thickness can be used to determine the growth rate of an early adult abalone shell.

Communicated by J. Grassle.

Electronic supplementary material The online version of this article (doi:10.1007/s00227-015-2615-y) contains supplementary material, which is available to authorized users.

S. Auzoux-Bordenave (✉) · A. Badou
UMR BOREA "Biologie des Organismes et Ecosystèmes Aquatiques", MNHN/CNRS 7208/IRD 207/UPMC, Muséum national d'Histoire naturelle, Station de Biologie Marine de Concarneau, 29900 Concarneau, France
e-mail: bordenav@mnhn.fr

S. Auzoux-Bordenave
Sorbonne Universités, UPMC, Université Paris 6, 4, place Jussieu, 75005 Paris, France

C. Brahmi
UMR EIO, Université de Polynésie française, BP 6570, 98702 Faa'a, French Polynesia

M. de Rafélis
UMR 7193 "Biominéralisations et Environnements sédimentaires", UPMC-ISTeP, 4, place Jussieu, 75005 Paris, France

S. Huchette
Ecloserie France-Haliotis, Kerazan, 29880 Plouguerneau, France

Introduction

The European abalone *Haliotis tuberculata* is a marine gastropod of economic interest and a model for studying basic mechanisms of mollusc shell formation. The calcareous abalone shell consists of two main biomineral layers underlying the periostracum, i.e. an outer prismatic layer and an inner nacreous layer. The nacre layer is made of highly ordered aragonite tablets (columnar) displaying remarkable mechanical properties and potential uses in jewellery and biomimetics (Jackson et al. 1990; Chateigner et al. 2000). While the nacreous layer is exclusively composed of aragonite, which is one of the $CaCO_3$ polymorphs, the mineralogical composition of the external shell layer may contain various proportions of aragonite and calcite depending on the species (Bøggild 1930; Mutvei et al. 1985; Dauphin et al. 1989). For instance, the external layer of *Haliotis asinina* adult shell is composed of 100 % aragonite, while the same layer is entirely made of calcite in the red abalone *H. rufescens* (Guo 2010). In the European abalone *H.*

tuberculata, the mineralogical composition of the external layer is still under debate. Indeed, previous studies reported either small amounts (<1 %) or no calcite in the shell (Bøggild 1930), while other studies reported a mixture of calcite and aragonite within the outer shell layer (Mutvei et al. 1985). Recent studies from our group on the microstructure (using SEM) and mineralogical composition (using FTIR) of the *H. tuberculata* shell from the early protoconch to the juvenile stage (Jardillier et al. 2008; Auzoux-Bordenave et al. 2010; Gaume et al. 2011) found that the early protoconch was mostly composed of amorphous calcium carbonate (ACC), while the shells of larval veligers to juveniles were essentially made of aragonite. Surprisingly, a more recent in situ analysis of the mature adult shell found a mixture of prismatic calcite and spherulitic-prismatic aragonite in the outer layer (Dauphin et al. 2014).

A major challenge in the field of biomineralisation is to relate the shell microstructure arrangement, the mineralogical and geochemical composition to shell growth dynamics. In the black-lip abalone *Haliotis rubra*, shell growth and microstructure were analysed by cathodoluminescence (CL) microscopy, electron microprobe analysis and Raman spectroscopy (Hawkes et al. 1996). Using labelling based on manganese (Mn) incorporation, the authors found CL bands of variable length and thickness behind the growing shell surface. Electron microprobe analysis of labelled shell layers confirmed that Mn concentrations within aragonite and calcite layers were associated with colour changes of the CL bands, respectively, yellow–green for aragonite and orange–red for calcite. Raman spectroscopy analysis confirmed the mineral nature of both prismatic and nacreous layers, while CL analysis showed that the mineralisation of calcite and aragonite may occur simultaneously in the outer prismatic layer. This showed that combining CL microscopy and spectroscopy analysis could be used to characterise the shell microstructure, the mineralogical composition and shell growth dynamics.

To complement this approach, chemical analysis of the shell allowed a better understanding of trace element changes and their relationships with the ultrastructure. For example, the ultrastructure components of the coral skeleton may have significant distinct geochemical signatures (Meibom et al. 2008). Although elemental (e.g. Mg/Ca, Sr/Ca) and isotopic ($\delta^{18}O$, $\delta^{13}C$, $\delta^{11}B$) compositions of coral skeletons have been widely used as proxies for (palaeo) environmental reconstructions, only a few studies have reported the relationships between trace element distributions and shell microstructure in molluscs (Gillikin et al. 2005), and their use as environmental proxies resulted in contradictory results (Carre et al. 2006). Heterogeneities observed in the biominerals within coral skeleton or mollusc shells are partly due to the control exerted by the organisms' physiology on chemical element incorporation and distribution into the carbonates, commonly referred to as the 'vital effect' (Weiner and Dove 2003). Indeed, the distribution of trace elements within the shell layers appears complex and is influenced by ontogeny, physiology and genetic controls as well as environmental conditions (Klein et al. 1996; Purton et al. 1999).

Trace element variations in mollusc shells have been previously attributed to kinetic effects (Lorrain et al. 2005), calcification rate, and/or variations in mantle tissue physiology (Purton-Hildebrand et al. 2001; Lazareth et al. 2007). Mineralogy was also shown to affect Sr incorporation in bivalve shell with aragonite typically containing twice as much Sr than calcite due to the difference in the crystal lattice of these two $CaCO_3$ polymorphs (Kinsman and Holland 1969; Gillikin et al. 2005). In abalone, only one study previously investigated the trace element composition in relation to shell growth and microstructure (Hawkes et al. 1996). Electron microprobe analysis of shell sections allowed measurement of levels of major (i.e. Ca) and trace elements (Mg, Fe, Sr, Mn) incorporated into both the calcite and aragonite shell layers of the abalone *Haliotis rubra*. While Mn concentrations were closely related to the CL-band intensity (and thus to the mineral structure), Ca and Sr levels within the shell layers showed no systematic relationship with the mineralogical nature of the layers (Hawkes et al. 1996). Investigation of trace element variations within the shell may provide new insights into organic–mineral interactions during mollusc shell biomineralisation and on the biological control of shell microstructure. Thus, further investigations at high spatial resolution are needed to specify the relationships between shell microstructure, mineral composition and trace element distribution in abalone shell.

Furthermore, many biomineralisation studies are primarily focused on the microstructure and composition of adult shell and the ontogenetic changes leading to the elaboration of a mature shell remain poorly documented. It is well known that significant morphological, microstructural and mineralogical changes occur during shell growth, from the early larval and juvenile stages to the formation of the composite bi-layered adult shell (Jackson et al. 2007; Auzoux-Bordenave et al. 2010). Controlled production of the European abalone *H. tuberculata* provides an opportunity to compare the microstructure, the mineralogical and geochemical composition of abalone shell at different growth stages.

In the present study, analyses were focused on metamorphic, postlarval, juvenile and early adult stages not previously examined. Shell microstructure, mineralogy and geochemical composition were investigated by scanning electron microscopy (SEM), Fourier transform infrared spectroscopy (FTIR) and ion microprobe analyses (NanoSIMS) to specify the temporal

and spatial distribution of the biominerals together with trace elements. A combination of manganese chloride ($MnCl_2$) labelling and cathodoluminescence observations was used to measure shell growth rate, giving new insights on the calcification dynamics over abalone shell development.

Materials and methods

Biological material

Haliotis tuberculata parental stock was collected on the northwest Brittany coast (Roscoff) and conditioned at the hatchery France-Haliotis (Plouguerneau, France) in flowing sea water. Larvae were obtained from controlled fertilisations in July 2009 and 2010 at a water temperature of 17 ± 0.5 °C. Larvae were sampled at a veliger stage 69 h postfertilisation, filtered on a 40-µm mesh filter and transferred to 15-mL tubes for further analysis. Ten-day postlarvae and 2-month juvenile abalones, grown on plates covered with microalgae, were detached with a pipette and sampled in 15-mL tubes for further analysis. Juvenile abalones grew in 1,000-L tanks where they were fed with green algae (*Ulvella lens and Ulva* sp.) until 8 months of age; at this time the diet was changed from green to red algae, *Palmaria palmata,* and juveniles were transferred to the open sea in cages. One-year-old abalones were obtained from open sea cages where they were fed with the red macroalga *P. palmata* for the last 4 months. For experimental Mn labelling, juvenile abalones were incubated for 2 h in sea water containing 90 mg L^{-1} of manganese chloride tetra-hydrate ($MnCl_2{\cdot}4H_2O$). The abalone shells were marked every 2 months from 6 week to 6 months. After the last Mn labelling, abalone were maintained in flowing sea water for 6 months to allow further shell deposition on top of the marked Mn-layer. Abalones were then dissected, and the shells were prepared for cathodoluminescence analyses.

Scanning electron microscopy (SEM)

After a 3 % glutaraldehyde fixation, larval and postlarval samples were dehydrated through a graded ethanol series and critical point dried with liquid carbon dioxide. Cross sections were obtained by cutting larval shells with a razor blade. For juvenile and adult abalone, soft tissue was removed by dehydration of the shell, cross sections were performed along the longitudinal axis. Samples were gold-coated (JEOL JFC 1200 fine coater) and observed at 5–15 kV with a JEOL JSM-840A scanning electron microscope (SEM, Service Commun de Microscopie Electronique, MNHN, Paris, France).

Fourier transform infrared spectroscopy (FTIR)

Larvae were fixed in 50 % ethanol and stored in 70 % ethanol until analysis. FTIR spectroscopy was performed on whole larval samples by direct attenuated total reflection (ATR) and on powdered samples mounted in KBr pellets according to a previously described method (Pichard and Fröhlich 1986; Gendron-Badou et al. 2003). For adult abalones, dried shells were cut along the longitudinal growth axis and embedded in Araldite 2020 (Huntsman). After a 48-h polymerisation at 37 °C, samples were polished at 3, 1 and 0.25 µm to eliminate streaks that can disrupt quality of FTIR analysis. FTIR-microscopy analyses were performed directly on shell sections. All spectra were obtained using a Brüker-Vector 22 FTIR spectrometer by accumulating 64 scans with a resolution of 2 cm^{-1} in the wavenumber range 2,000–650 cm^{-1}. The inner nacreous layer of adult abalone shell was used as a reference for further larval shell FTIR analysis. FTIR bands were interpreted according to the standard infrared transmission spectra of carbonate minerals (Jones and Jackson 1993).

Geochemical analysis using the NanoSIMS ion microprobe

Three to four samples of 69-h larvae and 10-day postlarvae, and one to two samples of 2-month juveniles and 1-year adults were analysed. A summary of the abalone specimens used and the number of shells analysed per stage are presented in Table 1 (ESM). Samples were cut along the growth longitudinal axis, embedded in Körapox® epoxy, and polished to 0.25 µm with a diamond suspension and gold-coated. Chemical mapping and spot analyses of trace element composition (i.e. Sr/Ca ratios) were carried out using a Cameca NanoSIMS ion microprobe at the Muséum national d'Histoire naturelle (Paris) following established procedures for biogenic carbonates (Meibom et al. 2008; Brahmi et al. 2010). Briefly, a primary beam of O^- delivered to the sample produced secondary ions of $^{44}Ca^+$ and $^{88}Sr^+$ that were transmitted to the mass spectrometer and detected simultaneously in electron multipliers at a mass resolving power of ~5,000. Line scans in spot mode (step size ~3 µm) and images of $^{88}Sr/^{44}Ca$ ratios were obtained by rastering the primary beam focused to about 300 nm spot size across a pre-sputtered surface to remove the gold-coating and establish sputtering equilibrium. Measured $^{88}Sr/^{44}Ca$ ratios obtained in spot mode were converted to molar ratios using the OKA-C carbonate standard analysed under identical conditions (Sr/Ca = 19.3 mmol mol^{-1}) from Bice et al. (2005). The external reproducibility of the Sr/Ca ratios of the standard was ~3 % (1 SD), respectively. Images of the $^{88}Sr/^{44}Ca$ ratios were obtained by combining five sequential, drift-corrected images of each isotope. Chemical maps were performed on all stages except for

the adult. Because the shells of young stages (i.e. 69 h and 10 days) were too thin, transect analyses in spot mode were only performed on juveniles and adult shells. To determine the variations of $^{88}Sr/^{44}Ca$ within early shells, line profiles were made on the chemical maps from the young stages. Data obtained from line profiles performed on chemical maps have no dimensions, while data obtained from transects in spot mode are expressed in mmol mol^{-1}.

Cathodoluminescence analysis

Samples cut along the longitudinal growth axis were embedded in Araldite 2020 epoxy (Huntsman) and polished to 0.25 μm using diamond suspensions. Shell sections of specimens labelled with Mn were observed under cathodoluminescence using an optical microscope coupled with a cold cathode device (Cathodyne-OPEA, 15–20 keV and 200–350 μA mm^{-2} under a pressure of 0.06 Torr). Digital images were obtained to observe the Mn-labelled increments mineralised using the method previously developed for bivalve shells (Lartaud et al. 2010; Mahé et al. 2010). Grey levels were extracted by image analysis using Image J software (http://rsbweb.nih.gov/ij/) measuring the luminous intensity of each pixel along a radial axis parallel to the growth axis. Grey peaks can be validated as labelled increments following simultaneously the grey-scale curve and its location along the main growth axis. Mn labelling was used as temporal point of reference to measure shell growth rate. The average daily shell growth rate was determined under an optical microscope from replicate measurements of the distance between the manganese mark and the shell surface ($n = 80$ measurements).

Results

Variations in the $^{88}Sr/^{44}Ca$ were investigated in parallel with the microstructure and mineral composition over abalone shell development. One-year abalone shells were used to determine shell growth rate from cathodoluminescence marks recorded following experimental manganese (Mn) incorporation.

Microstructure and trace element composition in the early developing shell

The microstructure and trace element composition of the abalone protoconch, from 69 h to 10 days, are presented (Fig. 1). As previously described (Auzoux-Bordenave et al. 2010), the mineralised protoconch of 69-h veliger larvae exhibited a uniform granular texture, without any sculptural pattern (Fig. 1a). The shell section revealed a thin mineralised layer, 2–3 μm thick, with irregular-shaped granules (Fig. 1b).

For the NanoSIMS chemical maps, blue indicates a lower Sr/Ca ratio than bright colours (orange–yellow). In the 69-h veliger shell, the chemical map of the $^{88}Sr/^{44}Ca$ ratio indicates that the Sr/Ca in the first 4 μm (starting from the inner part of the shell) was rather homogeneous and increased in the last micron of the outer part of the shell (Fig. 1c). The line profile of the chemical map from the inner to the outer shell confirmed the increase in the Sr/Ca ratio by a factor of ~1.5 in the outer part of the shell [Fig. 1d; Table 1 (ESM)].

After metamorphosis, the postlarval shell shows a well-defined transition between the original protoconch and the newly formed juvenile shell (Fig. 1e). A cross section in the late protoconch revealed three distinct mineralised layers: an inner and an outer prismatic layer, and a granular layer in between (Fig. 1f). The chemical map of the $^{88}Sr/^{44}Ca$ ratio showed a heterogeneous Sr concentration in the late protoconch related to its microstructure heterogeneity (Fig. 1g). The line profile starting from the inner part of the shell (black arrow Fig. 1g) confirmed this heterogeneous composition with a significant increase in the Sr/Ca ratio by a factor of 5 in the outer layer (Fig. 1h).

The microstructure and trace element composition of the newly formed juvenile shell were examined in 10-day and 2-month juvenile abalone (Fig. 2). The 10-day postlarva is a similar stage to the individual shown in Fig. 1e. The polished section of the postlarval stage indicates the two areas analysed with the ion microprobe in the protoconch (white-dotted box) and in the newly formed juvenile shell (black box) (Fig. 2a). A cross section of the newly formed juvenile shell showed a less defined 4-μm-thick crystalline layer compared to the protoconch (Fig. 2b). The chemical map of the $^{88}Sr/^{44}Ca$ ratio from the juvenile shell area (Fig. 2c) and a line profile performed on the chemical map revealed a rather homogeneous Sr composition from the inner (i) to the outer (o) shell (Fig. 2d; Table 1). A small region in the middle of the shell showed a lower $^{88}Sr/^{44}Ca$ ratio (by a factor 1.4) than the external parts of the shell (i.e. inner and outer parts). The 2-month juvenile abalone shell exhibited the typical ear shape and the growth rings of an adult shell (Fig. 2e) with the protoconch being enclosed by the new shell (arrowhead, Fig. 2e). The cross section through the juvenile shell showed a transition in crystalline microstructure, with minerals ordered in tablets within the inner layer (Fig. 2f). Chemical mapping of the $^{88}Sr/^{44}Ca$ ratio revealed a spatially heterogeneous Sr composition (Fig. 2g), which was confirmed by the spot analyses obtained from the transect shown in Fig. 2h. The inner part of the shell shows a quite homogeneous Sr/Ca ratio ranging from 1.8 to 4.5 mmol mol^{-1} along the inner 40–50 μm, while the outer part of the shell (15 μm thick) was characterised by

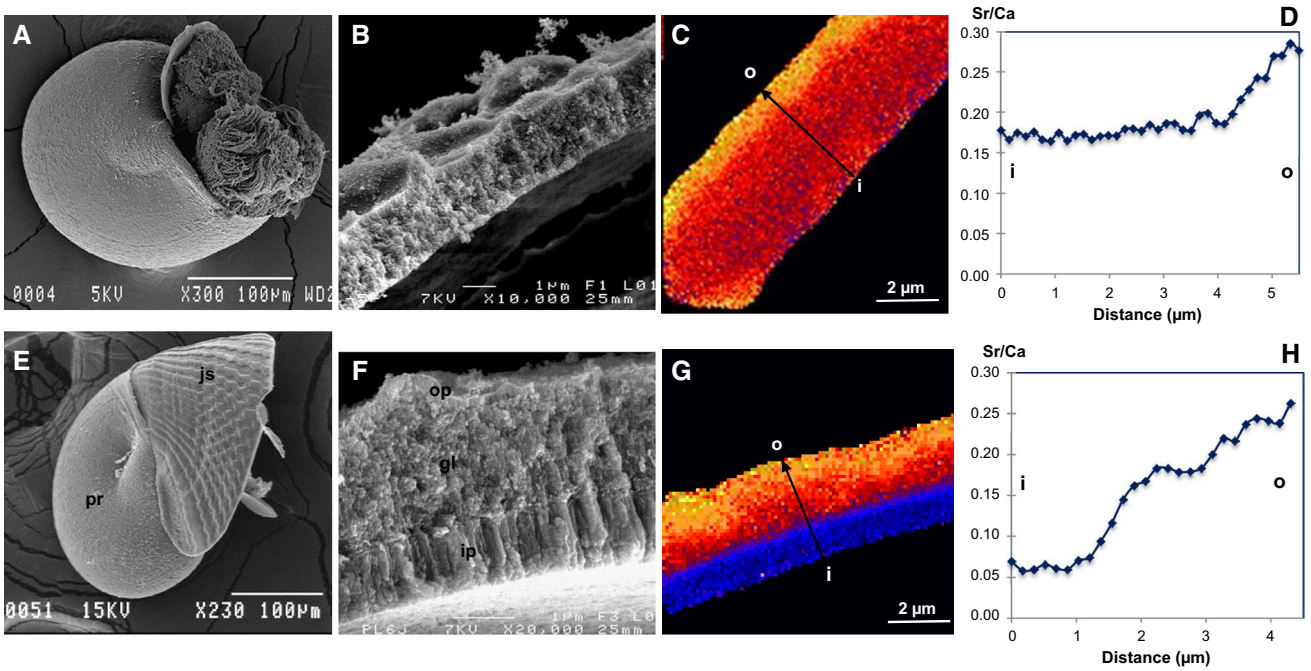

Fig. 1 Microstructure and trace element composition of abalone (*Haliotis tuberculata*) protoconch (69-h veliger and 10-day post-larva). **a** SEM of 69-h veliger. Larval shell with uniform granular texture. **b** Cross section of larval protoconch showing thin mineralised shell with poorly defined biominerals. **c** Chemical image of $^{88}Sr/^{44}Ca$ profile from inner (i) to outer (o) shell (*black arrow*) indicates homogeneous distribution of Sr in protoconch. **d** Line profile on chemical map reveals slight increase in Sr/Ca ratio in outer shell. **e** After metamorphosis, postlarval shell shows well-defined transition between protoconch (pr) and newly deposited sculptured, juvenile shell (js). **f** SEM of cross section of protoconch showing three crystalline layers: inner prismatic (ip), outer prismatic (op), and granular (gl) in between. **g** Chemical map of $^{88}Sr/^{44}Ca$ along transect (*black arrow*) reveals heterogeneous composition. **h** Line profile on this image (*black arrow* in **g**) confirming heterogeneous composition with increase in Sr/Ca ratio by a factor of 5 from inner (i) to outer (o) shell layer

a higher Sr/Ca ratio which gradually increased and reached a maximum of 6.8 mmol mol^{-1} [Fig. 2h; Table 1 (ESM)].

Microstructure, mineralogy and trace element composition in early adult abalone shell

Optical and SEM observations were made on 1-year abalone shells to characterise the changes in shell microstructure (Fig. 3). The length of cultured 1-year abalones is 14–18 mm ($n = 50$). The shell surface is brick-red and exhibits 8–9 open respiratory holes (Fig. 3a). A greenish-to-red colour transition is observed on the shell surface (Fig. 3a) as a consequence of the change in diet from green to red algae when juvenile abalones were transferred into open sea cages. This change in surface shell colour marks the transition between the juvenile and pre-adult stage. The larval protoconch is still visible at the origin and is enclosed within the juvenile shell. The inner surface of the abalone shell is made of an iridescent nacreous layer, and the nacre growth region has a dull appearance (Fig. 3b). The external layer has a granular structure, the nacreous layer a typical columnar structure and the thin inner layer (3–4 µm) is prismatic (Fig. 3c). The thickness of both external and nacreous layers varies along the section from 80 to 150 µm depending on the shell region, and the inner prismatic layer is not always observable. In some specimens, thin prismatic layers were interspersed within the nacreous layer (data not shown). The outer layer exhibits a homogeneous granular architecture, with biominerals lacking first-order structural arrangement (Fig. 3d), while the nacre cross section shows highly organised platelets of aragonite crystals stacked in a columnar structure (Fig. 3e). The nacre growth surface is characterised by confluent polygonal platelets, 6–8 µm in diameter (Fig. 3f). At higher magnification, the nacre surface shows the arrangement of aragonite platelets forming the typical stack of coins reported previously (Nakahara et al. 1982; Lin and Meyers 2005; Heinemann et al. 2011) in abalone nacre (Fig. 3g). Remnants of organic–mineral bridges were observed between the stacks.

FTIR spectroscopy and NanoSIMS analysis were performed on abalone shell cross sections along the longitudinal growth axis (Fig. 4a). The polished shell section used for mineralogical and geochemical analysis exhibits the typical bi-layered microstructure (Fig. 4b). Trace element analyses were performed on polished shell sections along a transect shown in Fig. 4c. Measured Sr/Ca ratios

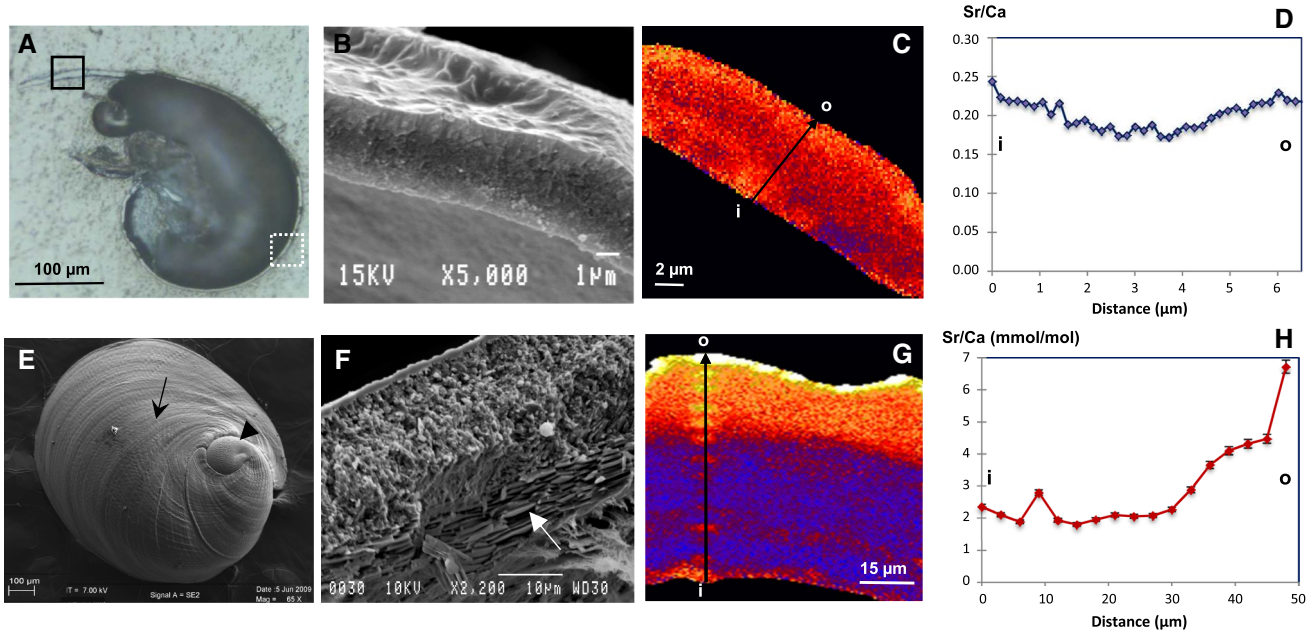

Fig. 2 Microstructure and trace element composition of the juvenile *Haliotis tuberculata* shell (10-days and 2-months). **a** Polished section of a 10-days shell indicating the two areas analysed using NanoSIMS in the protoconch (*white-dotted box*) and in the new juvenile shell (*black box*); **b** SEM of a cross section in the 10-day juvenile shell showing less defined crystalline layers. **c** Chemical image of $^{88}Sr/^{44}Ca$ ratio from the juvenile shell area (*boxed* in **a**) reveals a pretty homogeneous Sr concentration from inner (i) to outer (o) shell; **d** line profile performed on chemical image (*black arrow* in **c**) reveals a slight increase of 88Sr/44Ca ratio in outer shell; **e** SEM image of 2-month juvenile shell showing typical ear shape and growth rings (*arrow*); larval protoconch (*arrowhead*) is enclosed by juvenile shell; **f** SEM of cross section reveals a transition in crystalline microstructure, with minerals ordering in tablets within inner layer (*white arrow*). **g** Chemical map of $^{88}Sr/^{44}Ca$ ratio reveals a spatially heterogeneous composition in Sr trace element from inner (i) to outer (o) shell; **h** The inner shell shows a homogeneous composition in Sr with a Sr/Ca ratio averaging 2 mmol mol^{-1}, while outer part is characterised by a Sr/Ca ratio which gradually increases and reaches a maximum of 6.8 mmol mol^{-1}; *error bars* are SEM

(in spot mode) revealed a more homogeneous Sr concentration compared to the 2-month shell with an average of 1.85 ± 0.26 (RSD = 15 %) and small variations along the transect ranging from 1.4 (min. value) to 2.6 mmol mol^{-1} (max. value) [Fig. 4d; Table 1 (ESM)]. Starting from the inner part of the shell, the first 100 µm revealed a small and gradual decrease in Sr concentration. Then, over 15 µm a transition seemed to occur, after which the Sr/Ca ratio gradually increased up to one of the highest Sr/Ca values (2.5 mmol mol^{-1}). This transition seems correlated with the transition between the nacreous layer and the granular outer layer. Infrared spectra were obtained from four shell areas (Fig. 4e) and evidenced the five characteristic peaks of the aragonite polymorph of $CaCO_3$ (Fig. 4f).

Shell growth rate determined from Mn-labelling and cathodoluminescence analyses

Mn labelling was used as temporal point of reference to measure shell growth rate. Manganese uptake was detected on a polished cross section from a 1-year abalone shell (Fig. 5). The oblique axis along which the sections were made is shown in Fig. 5a. The protoconch is enclosed by the juvenile shell, the white arrow indicating the shell growth direction. A polished cross section of the shell along the oblique axis shows the protoconch in the middle, the juvenile shell on the left and the early adult shell on the right side (Fig. 5b).

The detail of the section, showing the different parts of the abalone shell, is shown in Fig. 5c. A cathodoluminescence image of the section (Fig. 5c) reveals a clear green band behind the growing surface (Fig. 5d). One to three CL bands could be distinguished according to the number of labelling events. The last Mn labelling performed on live 6-month abalones was used for the determination of shell growth rate (expressed in µm day^{-1}) by measuring the distance (d) between the Mn mark and the shell growing surface (Fig. 5e). The average shell growth rate, determined from different zones of the shell sections, was estimated at 0.35 µm day^{-1} ± 0.05 µm (n = 80 replicate measures pooled from three Mn-labelled shells).

Discussion

The present study investigated shell microstructure and composition in various stages of the abalone *Haliotis*

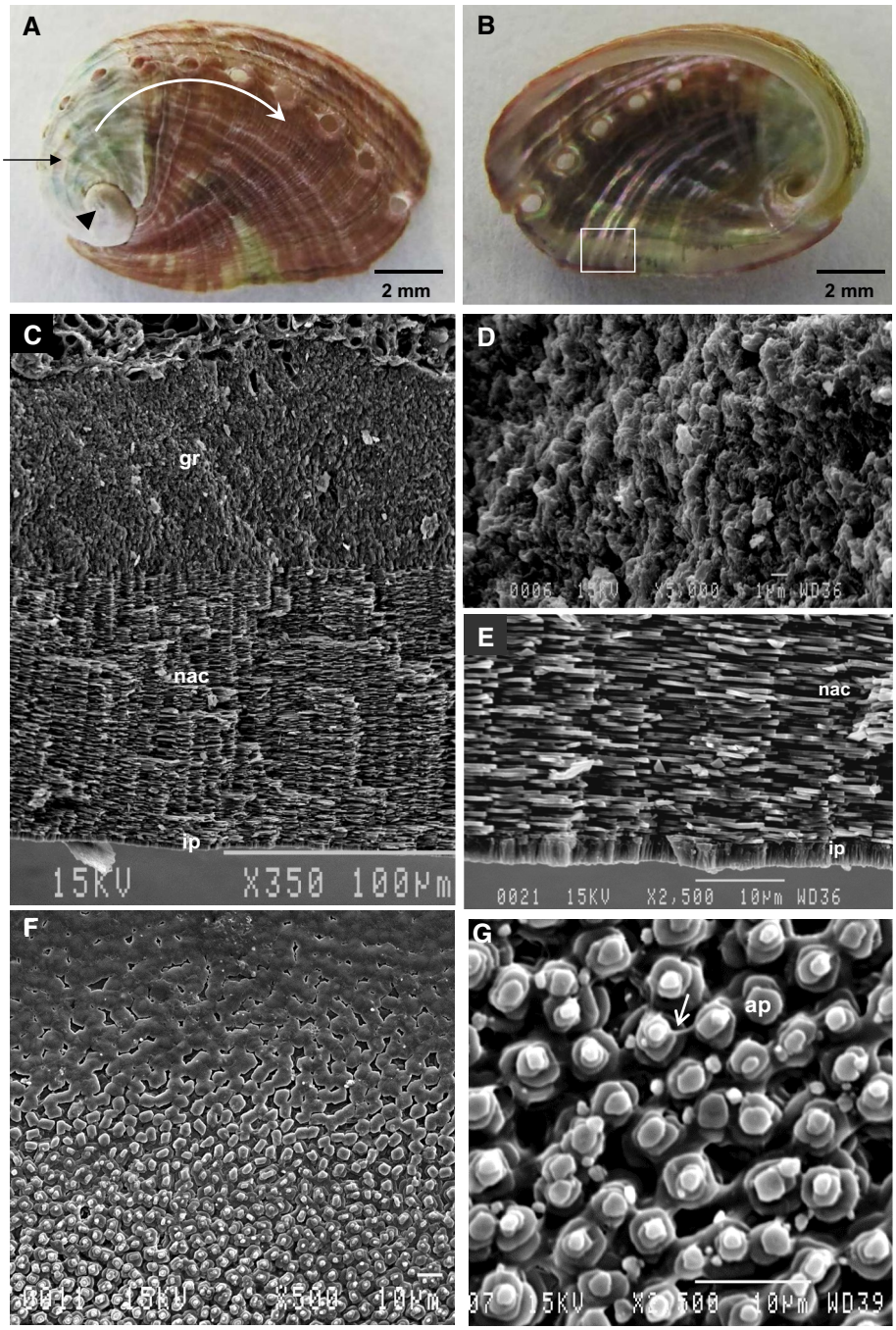

Fig. 3 Morphology and microstructure of early adult *Haliotis tuberculata* shell. **a** Shell of 1-year abalone is *red–brown* and exhibits 9–10 open respiratory holes; transition between juvenile and adult shell is marked by *greenish-to-red colour* change; protoconch is still visible at the origin (*arrowhead*) and is enclosed by juvenile shell (*black arrow*); *white arrow* indicates growth direction; **b** view of inner nacreous layer; **c** SEM of shell cross section showing outer granular layer (gr), nacreous layer (nac) and inner prismatic layer (ip); **d** SEM magnification of outer granular layer, showing biominerals lacking structural arrangement; **e** magnification of the nacreous layer (nac) showing arrangement of aragonite platelets and thin inner prismatic layer (ip); **f** SEM of the nacre growth region boxed in **b** showing confluent polygonal platelets; **g** magnification of nacre growth region shown in **f**: the arrangement of aragonite platelets (ap) form typical stack of coins linked with remnants of organic–mineral bridges (*white arrow*)

tuberculata to better understand the relationships between biomineral organisation, mineralogy and trace element composition throughout shell development. Furthermore, the combination of Mn labelling and CL microscopy allowed a determination of the growth rate of early adult shell (thickness).

SEM analysis of shell cross sections revealed a progressive biomineral organisation from the larval protoconch to the early juvenile stage, as previously described in *Haliotis tuberculata* (Auzoux-Bordenave et al. 2010). A well-defined shell microstructure was observed in 2-month juvenile shells with biominerals ordered in tablets in the inner layer, setting up the future nacreous layer of the early adult shell. In 1-year abalone shell, two to three distinct layers were observed, an outer granular layer, a nacreous layer and a very thin prismatic inner layer. Since the inner prismatic layer was not present in all specimens, or sometimes occurred inside the nacreous layer, it may be comparable to the growth lines previously described in *H. rufescens* and related to changes in environmental conditions,

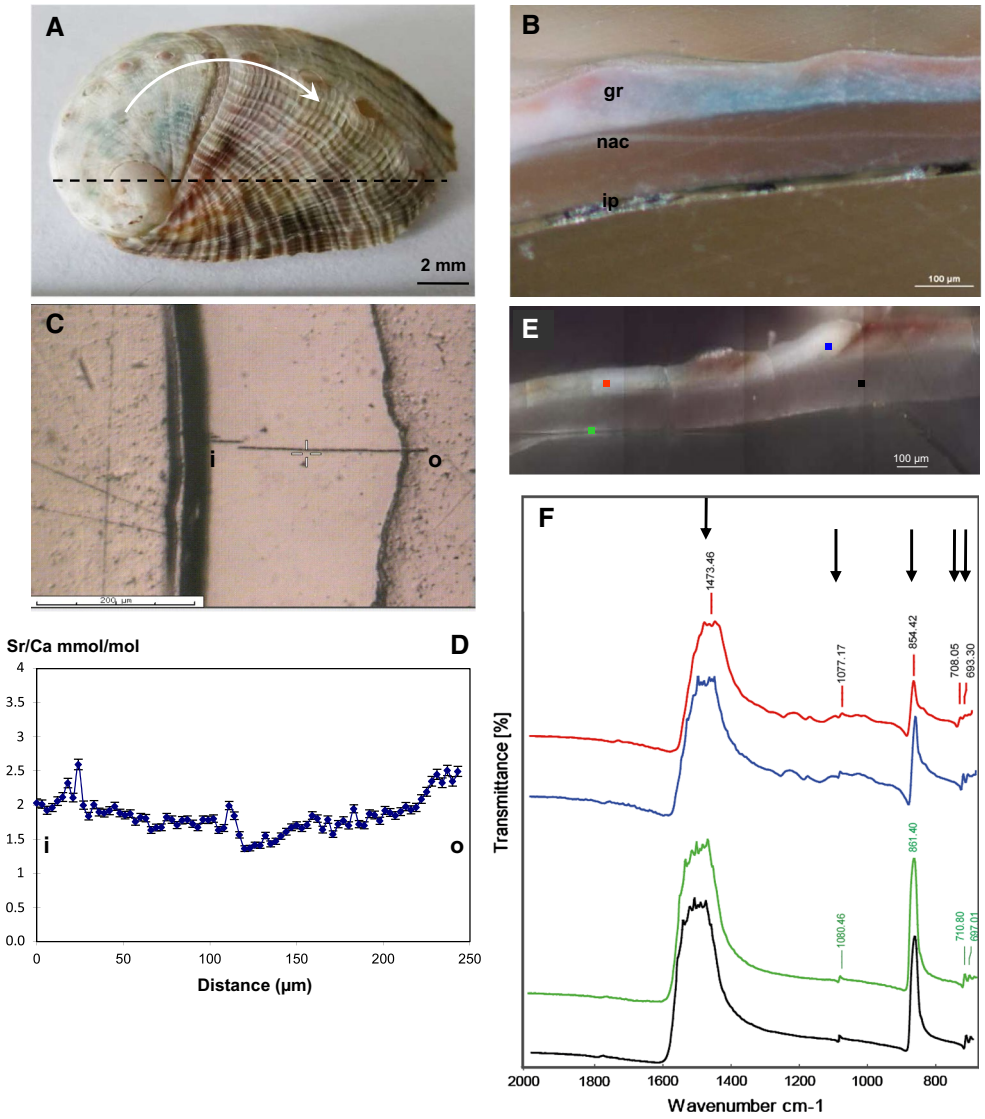

Fig. 4 Mineralogy and trace element composition of early adult *Haliotis tuberculata* shell. **a** External view of abalone shell showing longitudinal axis along which sections were made (*dotted line*); *white arrow* indicates shell growth direction; **b** polished cross section of adult shell showing three crystalline layers: outer granular layer (gr), nacreous layer (nac) and inner prismatic (ip); **c** polished section showing transect analysed with the ion microprobe from inner (i) to outer (o) shell; **d** variation of $^{88}Sr/^{44}Ca$ ratio along shell transect shown in **c**; *error bars* are SEM; **e**, **f** infrared spectra obtained from four areas within shell section (*squared* shown in **e**) showing five characteristic peaks of aragonite (*arrows*)

namely temperature (Su et al. 2002). The outer layer had a granular appearance where biominerals progressively assembled in the older shell to form the so-called spherulitic layer of the adult abalone shell (Lin and Meyers 2005). A cross section in the nacreous layer revealed the typical columnar organisation of abalone nacre, with nacre platelets ~8–10 µm in diameter, the growth morphology being very similar to that described earlier in other abalone species such as *H. laevigata* and *H. rufescens* (Nakahara et al. 1982; Heinemann et al. 2011).

FTIR spectra acquired from 1-year-old abalone shell indicated that the early adult shell of *Haliotis tuberculata* is mostly composed of the aragonite polymorph of $CaCO_3$. Aragonite was previously identified as the first mineral phase occurring in early abalone shell with an increase in the characteristic bands (700–712 and 853 cm^{-1}) from larval to juvenile shell (Auzoux-Bordenave et al. 2010). In the same way, aragonite appeared to be the only $CaCO_3$ polymorph in these *Haliotis tuberculata* shells at any stage of their development and we detected no calcite. These results contrast with recent data reported on the mineralogical composition of *Haliotis tuberculata* shells using high-resolution analysis, namely FTIR mapping combined with NanoSIMS analyses (Dauphin et al. 2014). In this paper,

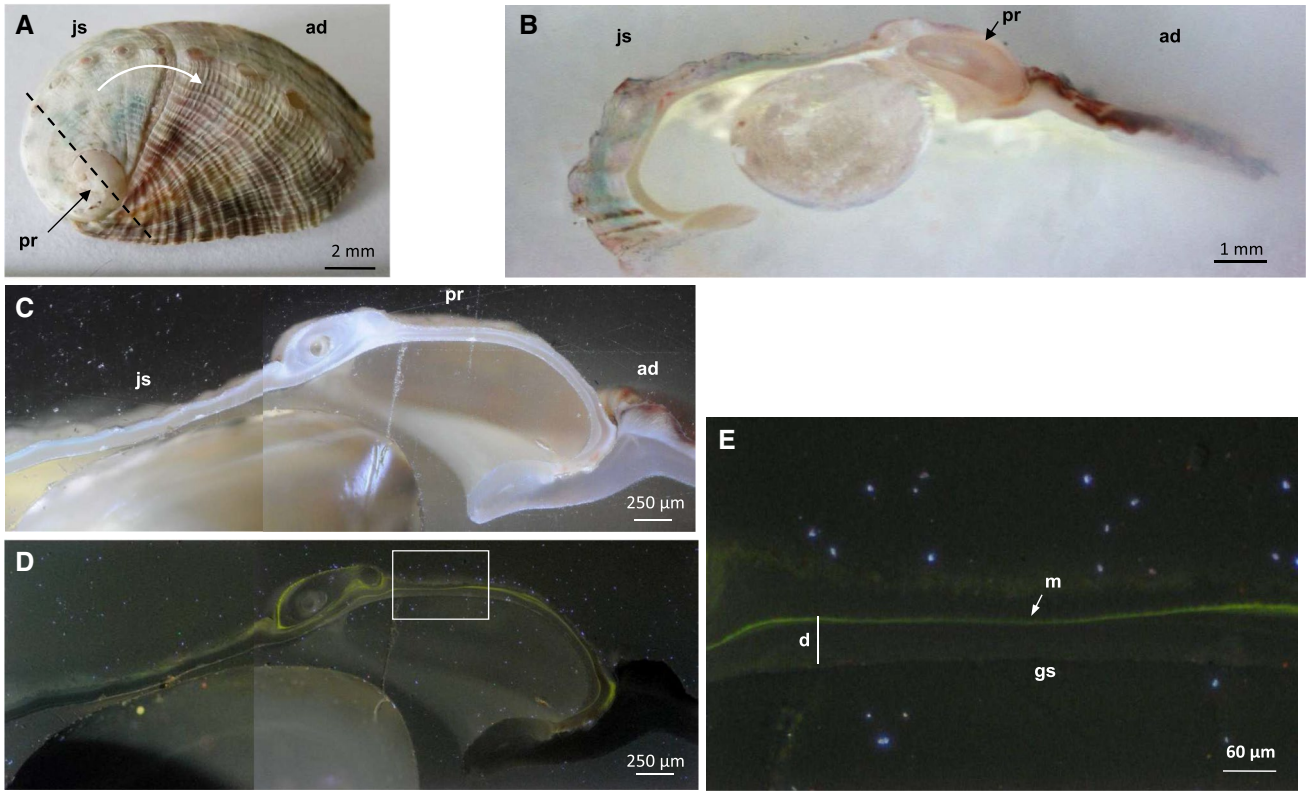

Fig. 5 In situ manganese uptake and shell growth evaluation in *Haliotis tuberculata*. **a** Photograph of a 1-year abalone shell showing oblique axis along which sections were made (*dotted line*); *white arrow* indicates shell growth direction, protoconch (pr), juvenile shell (js), early adult shell (ad); **b** polished cross section along the oblique axis shown in **a**; **c** detail of the section at higher magnification showing protoconch (pr) and new juvenile shell (js); **d** cathodoluminescence image of **c** showing *green line* resulting from the Mn-marking experiment. **e** Detail of shell area *boxed* in **d** showing Mn-labelled line (*green line* shown by *white arrow*). *Vertical white line* indicates the distance (d) between manganese mark (m) and shell growing surface (gs)

the authors reported the coexistence of large amounts of calcite with smaller aragonite patches within the outer layer in adult abalone. The differences between the two studies could be due either to individual variations within the abalone shell or to the higher resolution in the Dauphin et al. study (i.e. 5 × 5 µm compared to our 15 × 15 µm). Indeed, shell microstructure and composition may vary among populations due to various environmental conditions (personal observation). The difference in calcite composition in *H. tuberculata* in the present study and in Dauphin et al. (2014) might also be explained by the age of the abalone used for the analysis (1 year in our study and ~3 years in Dauphin et al.). It is interesting to note that in younger abalone specimens (present study), no calcite was detected. This observation raises questions about potential environmental and/or biotic factors that control the formation of $CaCO_3$ crystals by the gastropod.

Since Sr substitutes for Ca in the aragonite lattice, trace element analyses were focused on the $^{88}Sr/^{44}Ca$ ratio. This study describes for the first time variations in the Sr/Ca composition of abalone shell at different life stages in relation to its microstructure. Sr/Ca ratios measured in all abalone stages are within the broad range of Sr/Ca composition previously reported in mollusc shells (Carre et al. 2006; Lazareth et al. 2013). In abalone shell, Sr/Ca seems to be homogeneous when the shell layer is newly formed and not well organised (e.g. in the 69-h larvae and newly formed juvenile shells). In both postlarval and juvenile abalone shell, higher Sr/Ca ratios were found in the 'not well-defined' crystalline layers, while the lowest Sr/Ca ratio was measured in the inner well-defined crystalline layers. Since no changes in $CaCO_3$ polymorphs (mineralogy) were evident in the developing abalone shell, the variations in Sr concentration at a given stage may be attributed to microstructural changes occurring over the maturation of the aragonite lattice.

There are only a few studies on trace element incorporation into the larval shells of marine molluscs. Sr incorporation was shown to increase with temperature in the protoconch of the gastropod *Kelletia kelleti* (Zacherl et al. 2003). The results suggested the use of protoconch shell as proxies for environmental reconstructions, but the relationship

between trace element composition and shell microstructure was not investigated. In the developing abalone shell, the Sr/Ca ratio appeared significantly higher in juvenile than in adult shells. This is consistent with previous data showing that trace element incorporation varied with age in marine bivalves (Klein et al. 1996; Carre et al. 2006). Purton et al. (1999) reported an increase in Sr/Ca over bivalve shell growth inversely related to the calcification rate (i.e. Sr/Ca decreased with age). Variations in trace element concentrations were also observed in the shell of the gastropod *Concholepas concholepas* between day and night (Lazareth et al. 2007) and in various stages of the bivalve *Protothaca thaca* (Lazareth et al. 2013). In these examples, metabolic processes and/or calcification rate were thought to control element incorporation (Sr, Mg) through changes in the biological activity of the calcifying mantle (Carre et al. 2006; Lazareth et al. 2013). In the present study, the higher Sr/Ca ratio found in early abalone shell could be related to the higher calcification rate in the forming shell where crystal growth influences trace element concentration, especially Sr.

In abalone, there is only one previous study on trace element composition in relation to shell microstructure and mineralogy (Hawkes et al. 1996). Ca and Sr levels within the shell layers showed no systematic relationship with the mineralogical nature (calcite, aragonite) of the layers. In the present work, Sr/Ca ratio in early adult shell was quite homogeneous and exhibited only small decreases in the middle of the shell section. Although this slight decrease corresponded to the transition between the nacreous layer and the outer layer, the Sr/Ca composition in the adult shell cannot be directly related to heterogeneity in shell microstructure. But the homogeneous Sr composition is consistent with the aragonite nature of the shell layers.

The combination of manganese chloride ($MnCl_2$) labelling and cathodoluminescence observations on 1-year abalone allowed us to visualise the green CL bands characteristic of the aragonite polymorph. These results are consistent with previous data on the red abalone *H. rufescens*, showing that Mn incorporation was closely related to the mineral structure (Hawkes et al. 1996). In addition to FTIR spectroscopy analysis, these results confirm that the abalone shells were essentially composed of aragonite at every stage of their development. Manganese marks were used as a temporal reference to measure the rate at which abalone shell increased in thickness. The average shell growth rate, determined from different zones of abalone shell sections, was estimated at 0.35 µm $day^{-1} \pm 0.05$ µm. From our SEM observations of the shell sections, the increase in thickness from 6 to 12 months was estimated at 100–150 µm (data not shown), corresponding to 0.55–0.85 µm day^{-1}. Allowing for some uncertainty about shell section orientation, the shell growth rate calculated from cathodoluminescence marks is consistent with in situ measurements of shell thickness.

In the present study, Mn labelling of living abalones was performed at the end of March which corresponds to the beginning of active shell growth. The shell growth rate determined from CL marks in shell sections is also consistent with the growth dynamics previously reported for the European abalone (Clavier and Richard 1986; Roussel et al. 2011).

Our study brings new insights to the relationships between shell microstructure, shell growth and trace element distributions, especially Sr, over abalone development. Since the mineral composition of adult abalone (*Haliotis tuberculata)* shell is still under debate, additional high-resolution analysis would help specify the nature of the $CaCO_3$ polymorph (ACC, aragonite, calcite) in abalone shells of various ages and from different populations.

Acknowledgments This work was financed in part by the ATM program "Biomineralisation" of the MNHN funded by the Ministère délégué à l'Enseignement Supérieur et à la Recherche (Paris, France). We thank Pr Anders Meibom for the facilities and assistance for the NanoSIMS analysis ion microprobe (Muséum national d'Histoire naturelle, Paris, France). We are grateful to Claire E. Lazareth (UMR LOCEAN, Bondy, France) for her kind reading of the manuscript.

References

Auzoux-Bordenave S, Badou A, Gaume B, Berland S, Helléouet M-N, Milet C, Huchette S (2010) Ultrastructure, chemistry and mineralogy of the growing shell of the European abalone *Haliotis tuberculata*. J Struct Biol 171:277–290. doi:10.1016/j.jsb.2010.05.012

Bice KL, Layne GD, Dahl K (2005) Application of secondary ion mass spectrometry to the determination of Mg/Ca in rare, delicate, or altered planktonic foraminifera: examples from the Holocene, Paleogene, and Cretaceous. Geochem Geophys Geosyst 6:1–13. doi:10.1029/2005gc000974

Bøggild OB (1930) The shell structure of the mollusks. Det Kongelige Danske Videnskabernes Selskab Skrifter-Naturvidenskabelig og Mathematisk Afdeling 9:231–326

Brahmi C, Meibom A, Smith D, Stolarski J, Auzoux-Bordenave S, Nouet J, Doumenc D, Djediat C, Domart-Coulon I (2010) Skeletal growth, ultrastructure and composition of the azooxanthellate scleractinian coral *Balanophyllia regia*. Coral Reefs 29:175–189

Carre M, Bentaleb I, Bruguier O, Ordinola E, Barrett N, Fontugne M (2006) Calcification rate influence on trace element concentrations in aragonitic bivalve shells: evidences and mechanisms. Geochim Cosmochim Acta 70:4906–4920. doi:10.1016/j.gca.2006.07.019

Chateigner D, Hedegaard C, Wenk HR (2000) Mollusc shell microstructures and crystallographic textures. J Struct Geol 22:1723–1735

Clavier J, Richard O (1986) Growth of juvenile *Haliotis tuberculata* (Mollusca: Gastropoda) in their natural environment. J Mar Biol Assoc UK 66:497–503

Dauphin Y, Cuif J-P, Mutvei H, Denis A (1989) Mineralogy, chemistry and ultrastructure of the external shell-layer in ten species of *Haliotis* with reference to *Haliotis tuberculata* (Mollusca: Archaeogastropoda). Bull Geol Inst Univ Uppsala 15:7–38

Dauphin Y, Cuif J-P, Castillo-Michel H, Chevallard C, Farre B, Meibom A (2014) Unusual micrometric calcite–aragonite interface

in the abalone shell *Haliotis* (Mollusca, Gastropoda). Microsc Microanal 20:276–284. doi:10.1017/S1431927613013718

Gaume B, Fouchereau-Peron M, Badou A, Helléouet M-N, Huchette S, Auzoux-Bordenave S (2011) Biomineralization markers during early shell formation in the European abalone *Haliotis tuberculata*, Linnaeus. Mar Biol 158:341–353. doi:10.1007/s00227-010-1562-x

Gendron-Badou A, Coradin T, Maquet J, Fröhlich F, Livage J (2003) Spectroscopic characterization of biogenic silica. J Non-Cryst Solids 316:331–337

Gillikin DP, Lorrain A, Navez J, Taylor JW, André L, Keppens E, Baeyens W, Dehairs F (2005) Strong biological controls on Sr/Ca ratios in aragonitic marine bivalve shells. Geochem Geophys Geosyst 6:1–15

Guo D-J (2010) Microstructure and crystallography of abalone shells. Thesis, Research Master Degree, Glasgow

Hawkes GP, Day RW, Wallace MW, Nugent KW, Bettiol AA, Jamieson DN, Williams MC (1996) Analyzing the growth and form of mollusc shell layers, in situ, by cathodoluminescence microscopy and Raman spectroscopy. J Shellfish Res 15:659–666

Heinemann F, Launspach M, Gries K, Fritz M (2011) Gastropod nacre: structure, properties and growth: biological, chemical and physical basics. Biophys Chem 153:126–153. doi:10.1016/j.bpc.2010.11.003

Jackson A, Vincent J, Turner R (1990) Comparison of nacre with other ceramic composites. J Mater Sci 25:3173–3178

Jackson DJ, Wörheide G, Degnan BM (2007) Dynamic expression of ancient and novel molluscan shell genes during ecological transitions. BMC Evol Biol 7:160. doi:10.1186/1471-2148-7-160

Jardillier E, Rousseau M, Gendron-Badou A, Fröhlich F, Smith D, Martin M, Helléouet M-N, Huchette S, Doumenc D, Auzoux-Bordenave S (2008) A morphological and structural study of the larval shell from the abalone *Haliotis tuberculata*. Mar Biol 154:735–744

Jones GC, Jackson B (1993) Infrared transmission spectra of carbonate minerals. Chapman & Hall, London

Kinsman DJJ, Holland HD (1969) Co-precipitation of cations with CaCO3 IV. Co-precipitation of Sr^{2+} with aragonite between 16° and 96°C. Geochim Cosmochim Acta 33:1–17

Klein RT, Lohmann KC, Thayer CW, January R (1996) Sr/Ca and $^{13}C/^{12}C$ ratios in skeletal calcite of *Mytilus trossulus*: covariation with metabolic rate, salinity and carbon isotopic composition of seawater. Science 60:4207–4221

Lartaud F, de Rafelis M, Ropert M, Emmanuel L, Geairon P, Renard M (2010) Mn labelling of living oysters: artificial and natural cathodoluminescence analyses as a tool for age and growth rate determination of *C. gigas* (Thunberg, 1793) shells. Aquaculture 300:206–217. doi:10.1016/j.aquaculture.2009.12.018

Lazareth CE, Guzman N, Poitrasson F, Candaudap F, Ortlieb L (2007) Nyctemeral variations of magnesium intake in the calcitic layer of a Chilean mollusk shell (*Concholepas concholepas*, Gastropoda). Geochim Cosmochim Acta 71:5369–5383

Lazareth CE, Le Cornec F, Candaudap F, Freydier R (2013) Trace element heterogeneity along isochronous growth layers in bivalve shell: consequences for environmental reconstruction. Palaeogeogr Palaeoclimatol Palaeoecol 373:39–49. doi:10.1016/j.palaeo.2011.04.024

Lin A, Meyers MA (2005) Growth and structure in abalone shell. Mat Sci Eng A 390:27–41

Lorrain A, Gillikin DP, Le Mercier A (2005) Strong kinetic effects on Sr/Ca ratios in the calcitic bivalve *Pecten maximus*. Geology 12:965–968

Mahé K, Bellamy E, Lartaud F, de Rafélis M (2010) Calcein and manganese experiments for marking the shell of the common cockle (*Cerastoderma edule*): tidal rhythm validation of increments formation. Aquat Living Res 23:239–245. doi:10.1051/alr/2010025

Meibom A, Cuif J-P, Houlbreque F, Mostefaoui S, Dauphin Y, Meibom KL, Dunbar R (2008) Compositional variations at ultrastructure length scales in coral skeleton. Geochim Cosmochim Acta 72:1555–1569

Mutvei H, Dauphin Y, Cuif J-P (1985) Observations sur l'organisation de la couche externe du test des *Haliotis* (Gastropoda): un cas exceptionnel de la variabilité minéralogique et microstructurale. Bulletin du Muséum national d'Histoire naturelle, Paris, 4e série 7, section A, 1:73–91

Nakahara H, Bevelander G, Kakei M (1982) Electron microscopic and amino acid studies on the outer and inner shell layers of *Haliotis rufescens*. Venus (Japan J Malacol), pp 33–46

Pichard C, Fröhlich F (1986) Analyses infrarouges quantitatives des sédiments. Exemple du dosage du quartz et de la calcite. Revue de l'Institut français du Pétrole 41:809–819

Purton L, Shields G, Brasier M, Grime G (1999) Metabolism controls Sr/Ca ratios in fossil aragonitic mollusks. Geology 27:1083–1086

Purton-Hildebrand LMA, Shields GA, Brasier MD (2001) The use of external micro-PIXE to investigate the factors determining the Sr:Ca ratio in the shells of fossil aragonitic molluscs. Science 181:506–510

Roussel S, Huchette S, Clavier J, Chauvaud L (2011) Growth of the European abalone (*Haliotis tuberculata* L.) in situ: seasonality and ageing using stable oxygen isotopes. J Sea Res 65:213–218. doi:10.1016/j.seares.2010.10.001

Su X, Belcher AM, Zaremba CM, Morse DE, Stucky GD, Heuer AH (2002) Structural and microstructural characterization of the growth lines and prismatic microarchitecture in red abalone shell and the microstructures of abalone "flat pearls". Chem Mater 14:3106–3117

Weiner S, Dove PM (2003) An overview of biomineralization processes and the problem of the vital effect. In: Dove PM, De Yoreo JJ, Weiner S (eds) Biomineralization. American Mineralogical Society, Washington, DC, pp 1–29

Zacherl DC, Paradis G, Lea DW (2003) Barium and strontium uptake into larval protoconchs and statoliths of the marine neogastropod *Kelletia kelletii*. Geochim Cosmochim Acta 67:4091–4099